STRUCTURAL FEATURES OF BREAKING WAVES IN STRATIFIED FLOW OVER MOUNTAINS

O. EIFF[1], P. BONNETON[2]
[1] *Centre National de Recherches Météorologiques de Toulouse, Météo-France, 42 av G. Coriolis, 31057 Toulouse, France.*
[2] *Département de Géologie et Océanographie, Université Bordeaux 1, av des Facultés, 33405 Talence, France.*

1. Introduction

When internal waves generated by flow over mountains break under sufficiently stably stratified atmospheric conditions, a localized turbulent zone is created. This is one important example of the mechanisms which engender so-called 'clear air turbulence'. The presence of a turbulent zone is a concern for air traffic and the associated increase in wind trapped between this turbulent zone and the mountain creates strong storms on the lee-side of the mountain. Furthermore, this phenomenon increases the drag on the atmosphere which needs to be accounted for in numerical weather prediction models.

Considerable numerical and theoretical research on mountain-wave breaking has focused on the increase in wave surface-drag and the generation of severe windstorms [e.g., Klemp & Lilly (1975), Peltier & Clark (1979,1983), Clark & Peltier (1977), Clark & Farley (1984) and later Smith (1985, 1991)]. The laboratory experiments by Rottman & Smith (1989) also studied the generation of severe windstorms, and were extended by Castro & Snyder (1993) to include the effect of the hill shape on the range of Froude numbers leading to wave-breaking. The dynamics of the mountain-wave breaking process itself, on the other hand, was investigated by Laprise & Peltier (1989a, 1989b) via two-dimensional linear stability analysis and numerical simulation, and more recently by Afanasyev & Peltier (1998) via a three-dimensional simulation.

A central focus of the recent studies on the dynamics of internal-wave breaking, which include wave breaking in critical layers [e.g., Winters & Riley (1992) and Andreassen *et al.* (1998)], is the determination of the

type of instability mechanism which generates wave breaking. The three-dimensional numerical simulation results by Afanasyev & Peltier (1998) on mountain-wave breaking have shown that streamwise vortices are created in the wave breaking region by a shear-aligned convective instability, as previously observed in the cores of Kelvin-Helmholtz billows. All studies found that three-dimensional effects play a central role in the development of the convective instabilities and thus have to be considered. The present work aims to detail the evolution leading to mountain-wave breaking and the resulting vortical structures, as observed in the laboratory. Emphasis will be given on the three-dimensional structures generated by quasi two-dimensional mountains.

2. Experimental Method

Quasi two-dimensional Gaussian-shaped obstacles or 'mountains', of cross-sectional shape $h(x) = H \exp(-x^2/2L^2)$ where H is the height of the mountains and L the characteristic streamwise length, were towed at uniform velocity U in linearly stratified saline solutions of Brunt-Väisälä frequency N of approximately one rad/sec (see figure 1). The quasi two-dimensional mountains are uniform along the spanwise direction for a length W. The ends of the mountains are smoothed by the same Gaussian shape as in the streamwise direction and in a semi-circular manner. While more representative of actual mountain ranges, towing quasi two-dimensional mountains rather than two-dimensional mountains also reduces the upstream perturbations due to blocking at low Froude numbers.

In order to examine three different Reynolds number ranges, $Re = UH/\nu \sim \{10^2, 10^3, 10^4\}$, the experiments were carried out with three different size models in three corresponding tanks of size $(H_t \times W_t \times L_t)$ equal to 0.5 x 0.5 x 4m^3, 0.7 x 0.8 x 7m^3 and 1.5 x 3.0 x 22m^3. The models were scaled such that the vertical and spanwise confinement effects in each tank were the same, specifically, $H/L = 0.57$, $W/H = 10.3$ and $W/W_t = 0.45$. The mountains were towed in an upright configuration at the bottom of the tanks, suspended by thin metal threads in order to avoid perturbations generated by the baseplate of an upside-down configuration [e.g., Castro & Snyder (1993)].

The flow is essentially governed by three parameters, the vertical Froude number, $F_v = U/NH$, a measure of the non-linear effects, the horizontal Froude number, $F_h = U/NL$, a measure of the non-hydrostatic effects, and the Reynolds number. The present experiments were all performed in the non-linear regime where wave breaking occurs, at $F_v = 0.6$ with $F_h = F_v H/L = 0.34$.

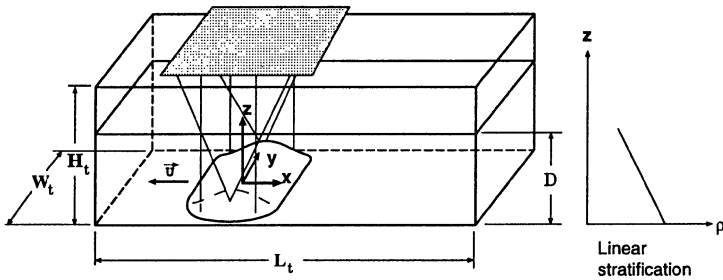The flow was examined with particle tracking as well as fluorescent-dye

Figure 1. Experimental setup

imaging methods. Laser-light sheets were used to illuminate the particles and/or the fluorescent dye in given cross-sectional planes of the flow. The particles used were neutrally buoyant and spanned the density range of interest. The flow was recorded on S-VHS tape for subsequent digital processing and analysis.

3. Temporal evolution

Figure 2 shows the streakline pattern obtained in the vertical center plane of the flow for several non-dimensional times (Nt) as the wave develops. The wave is observed to steepen [figure 2(a)] and eventually reaches the critical condition for static instability near $Nt = 28$ [figure 2(b)]. However, rather than becoming immediately unstable, the flow continues to remain dynamically stable for several buoyancy periods, folding into an 'S'-shape [figure 2(c)]. Such dynamic stability has also been observed in other wave-breaking situations such as oscillating tubes [Thorpe (1994)]. The upper half of the 'S' wave pinches faster than the lower one, resulting, a few buoyancy periods later, at $Nt = 48$, in a clockwise rotating vortex [figure 2(d)]. This configuration continues to evolve more rapidly than before into a counter-rotating vortex pair by $Nt = 54$ [figure 2(e)]. In accordance with the generation of lee-side windstorms under wave-breaking conditions [e.g., Peltier and Clark (1979)], the maximum velocity in the lower level jet-like flow has accelerated from about $2.0U$ when the wave is critical to about $2.2U$ when the counter-rotating vortex pair has formed.

The subsequent flow evolution remains unsteady and is accompanied by complete changes in topology. Whereas the flow at $Nt = 54$ was characterized by four critical points (two counter-rotating foci and two saddle points), a topology with no critical points occasionally appears at later times [e.g., figure 2(f)]. This apparent 'relaminarization' has bifurcation lines and is therefore three-dimensional. In contrast, the earlier steepening wave reveals no bifurcation lines, implying that the flow can be two-dimensional.
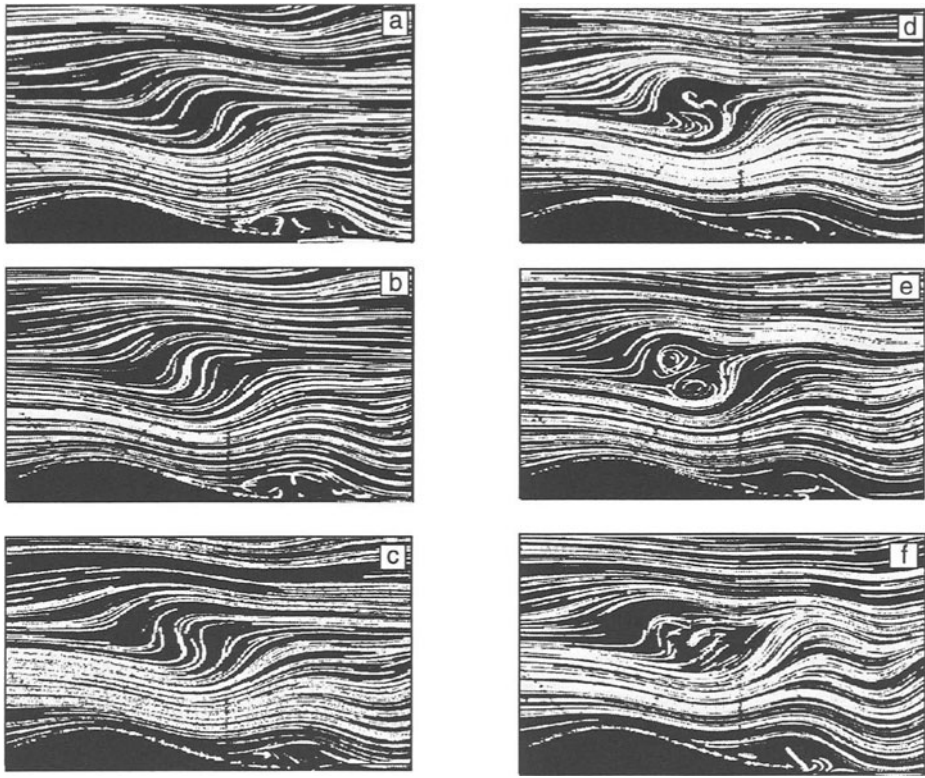
Figure 2. Streaklines in the $y = 0$ vertical plane at $Re = 130$. (a) $Nt = 26$, (b) $Nt = 28$, (c) $Nt = 44$, (d) $Nt = 48$, (e) $Nt = 54$, (f) $Nt = 150$. The flow is from left to right.

Similar experiments were carried out for the three Reynolds number ranges. The same evolution was observed, although it is increasingly rapid as the Reynolds number increases.

It can be noted that there are some differences between the tank experiments and the series of inviscid numerical simulations such as those of Peltier and Clark (1979) or Afanasyev and Peltier (1998), in which a downward and downstream penetration of the turbulent breaking zone was observed. While our own series of numerical simulations (Gheusi et al. 1999), in similitude with the experiments, revealed a similar downward and downstream penetration when surface friction was not taken into account, simulations with surface friction revealed close agreement with the experiments. Allowing for surface friction thus appears to generate the flow separation on the lee side of the mountain surface with a strong trapped lee-wave (figure 2), which, in turn, prevents the downstream propagation of the wave-breaking region and effectively confines the breaking zone.

4. Transverse vortex

The above results suggest that at some point in the evolution of the flow, the structural features of the flow become three-dimensional. Recent numerical simulations [e.g., Winters & Riley (1992)] have shown that three-dimensionality is an essential characteristic for convective instability. Therefore, in order to examine the three-dimensional aspects, the flow was viewed simultaneously in two orthogonal planes, the vertical $x - z$ plane and the horizontal $x - y$ plane. The horizontal laser sheet was positioned at the center of the wave breaking region ($z/H = 2.5$) and the vertical sheet at $y = 0$.

Simultaneously sampled particle tracking results are presented in figure 3 for $Re = 580$ at $Nt = 32$. The vertical plane in figure 3(a) clearly shows a clockwise vortex which was also observed in figure 2(d) at lower Re. Although the streaklines in the horizontal plane [figure 3(b)] reveal bifurcation lines, the flow is still quasi two-dimensional over the center of the mountain, spanning about 50% of the homogeneous section. It can therefore be deduced that the clockwise vortex identified in the vertical plane represents a cross-sectional view of a structure with significant transverse extent. The bifurcation lines are due to slight deviations from perfect spanwise alignment. The existence of a clockwise vortex with transverse extent is further supported by observations of similar clockwise vortices in the off-center vertical plane at $y/H = 3$ and by the fact that such vortices were consistently observed when the experiments were repeated.
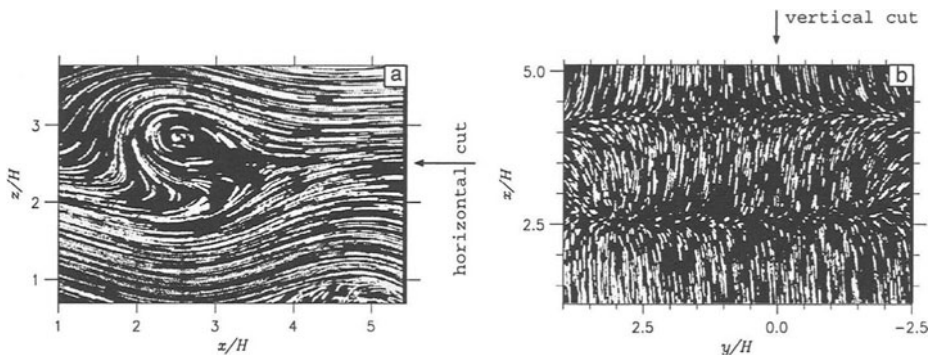

Figure 3. Simultaneous particle tracking results at $Re = 580$ and $Nt = 32$. (a) Vertical $x - z$ plane at $y = 0$; (b) horizontal $x - y$ plane at $z/H = 2.5$

The formation of a transverse vortex is characteristic of a shear instability. This is consistent with measurements of the gradient Richardson number, $Ri = N^2(du/dz)^{-2}$, which is less than 0.25 in a narrow band above

the statically unstable region, although this criterion is strictly only valid for parallel and inviscid flow.

5. Toroidal vortices

The subsequent development is highly three-dimensional across the entire mountain ridge. The two different topologies that appear in the vertical plane [figures 2, (e, f)] can be explained if the underlying structures in the wave breaking region were to consist of toroidal vortices inclined into the flow as depicted in figure 4. A vertical cross-section through the center of one toroidal vortex would result in the counter-rotating vortex pair observed in figure 2(e). The flow between two adjacent structures, in the absence of smaller scale structures, would appear as the 'relaminarized' flow with bifurcation lines as seen in figure 2(f). Lateral advection of such structures would cause these two topologies to be observed in a fixed plane at different times.
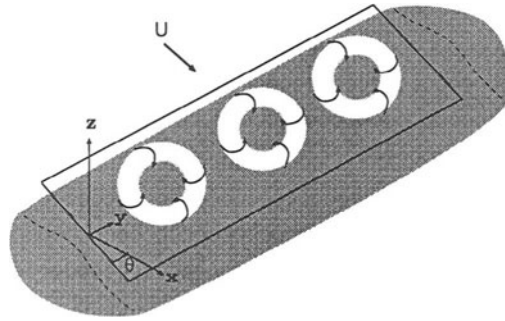

Figure 4. Vortex skeleton model of the large-scale structures in the wave-breaking region. The co-rotating structures are inclined with respect to the horizontal.

Two simultaneously acquired cross-sectional planes at two such different times are shown in figures 5(a)-(d). Figure 5(a), at $Nt = 64$, reveals a flow without critical points in the $y = 0$ plane, while in the vertical plane [figure 5(b)] several adjacent counter-rotating vortex pairs can be identified. Clearly, the flow is not two-dimensional anymore and the counter-rotating vortex pairs seen in figure 5(b) are to be expected from inclined toroidal vortices intersected in the horizontal plane. Taking into account the senses of rotation of the vortices, one can identify two such counter-rotating vortex pairs which are centered about $y = 0$. Given that two vortex pairs are centered about $y = 0$, no critical points are expected in the $y = 0$ vertical plane, which is verified by the results shown in figure 5(a).

At a later time ($Nt = 128$), one vortex pair remains in the horizontal plane shown in figure 5(d). Since the vortex is centered at $y = 0$, we expect a

counter-rotating vortex to appear in the $y = 0$ vertical plane - as can be seen in figure 5(c). Thus, these measurements confirm the topological features expected from the presence of toroidal vortices in the flow. These vortices are strongly inclined with respect to the horizontal direction, yielding both longitudinal and vertical vorticity in addition to transverse vorticity.
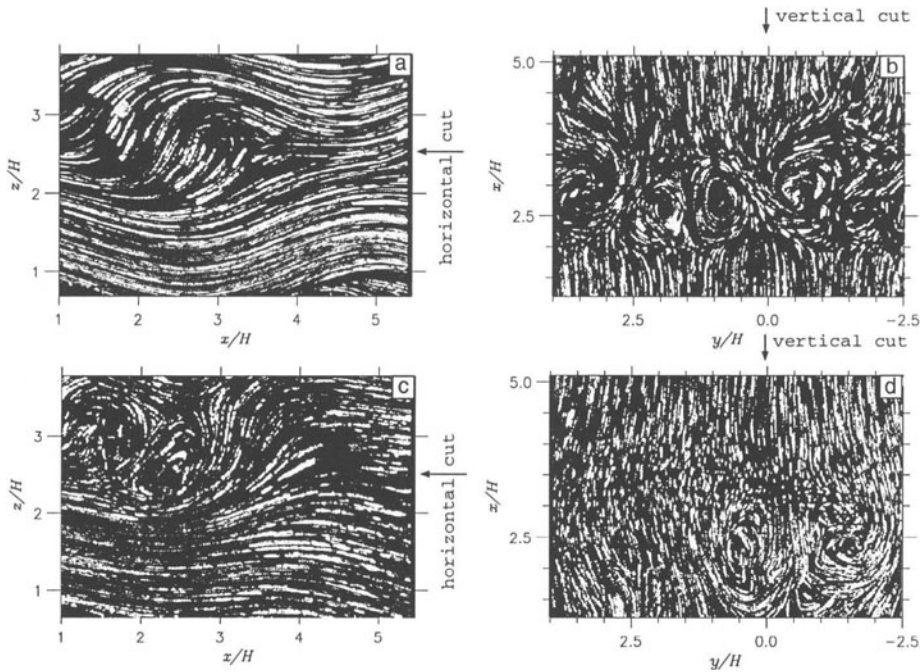

Figure 5. Simultaneous particle tracking results at $Re = 580$ at two different times. (a) $x - z$ plane at $y = 0$, $Nt = 64$; (b) $x - y$ plane at $y/H = 2.5$, $Nt = 64$; (c) $x - z$ plane at $y = 0$, $Nt = 128$; (d) $x - y$ plane at $y/H = 2.5$, $Nt = 128$.

6. Discussion and conclusion

Toroidal vortices with significant components of vorticity in all directions have been shown to exist within the localized zone of breaking waves over quasi two-dimensional mountains. The scale of these vortices is about $1.5H$ in all directions. Clearly, these vortices are expected to play a major role in the mixing efficiency and turbulence characteristics of wave breaking.

The longitudinal component of vorticity due to the toroidal vortices also consists of counter-rotating vortex pairs. Generation of such longitudinal counter-rotating vortices is commonly associated with three-dimensional convective instabilities [e.g., Winters & Riley (1992), Andreassen *et. al.*

(1998), and Afanasyev & Peltier (1998)]. It thus appears that three-dimensional convective instability, at least over the central homogeneous portion of the mountain, does not set in until a transverse vortex has been formed by two-dimensional shear instability. The reason is likely to be that the wave-generated shear will tend to dampen convective instability in the form of longitudinal vorticity in the initial stages, as demonstrated by Deardorff (1965).

7. Acknowledgments

8. References

Afanasyev, Y. D. & Peltier, W.R. 1998 The three-dimensionalization of stratified flow over two-dimensional topography. *J. Atmos. Sci.* **55**(1), 19-39.

Andreassen, O., Hvidsten, P.O., Fritts, D.C. & Arendt S. 1998 Vorticity dynamics in a breaking internal gravity wave. Part 1. Initial instability evolution. *J. Fluid Mech.* **367**, 27-46.

Castro, I.P. & Snyder W.H. 1993 Experiments on wave breaking in stratified flow over obstacles. *J. Fluid Mech.*, **225**, 195-211.

Clark, T.L., & Farley, R.D. 1984 Severe downslope windstorms calculations in two and three spatial dimensions using anelastic interactive grid nesting: a possible mechanisms for gustiness. *J. Atmos.Sci*, **43** No.3, 329-350.

Clark, T.L., & Peltier, W.R. 1977 On the evolution and stability of finite-amplitude mountain waves. *J. Atmos. Sci*, **34**, 1715-1730.

Deardorff, J.W. 1965 Gravitational instability between horizontal plates with shear. *Phys. Fluids*, 8(6), 1027-1030.

Gheusi, F., Stein, J. & Eiff, O.S. 1999 A numerical study of three-dimensional orographic gravity-wave breaking observed in a hydraulic tank. Submitted to *J. Fluid Mech.*

Klemp, J.B. & Lilly, D.K. 1975 The dynamics of wave induced downslope winds. *J. Atmos. Sci*, **32**, 320-339.

Laprise, R. & Peltier W.R. 1989a The linear stability of non-linear mountain waves: implications for the understanding of severe downslope windstorms. *J. Atmos. Sci*, **46**, 545-564.

Laprise, R. & Peltier W.R. 1989b The structure and energetics of transient eddies in a numerical simulation of breaking mountain waves. *J. Atmos. Sci*, **46**, 586-585.

Peltier, W.R. & Clark, T.L. 1979 The evolution and stability of finite-amplitude mountain waves. Part II: Surface wave drag and severe downslope windstorms. *J. Atmos. Sci*, **36**, 1498-1529.

Peltier, W.R. & Clark, T.L. 1983 Nonlinear mountain waves in two and three spatial dimensions. *Quart. J. R. Met. Soc.*, **109**, 527-548.

Rottman, J.W. & Smith, R.B. 1989 A laboratory model of severe downslope winds. *Tellus*, **41A**, 401-415.

Smith, R.B., 1991 Kelvin Helmholtz instability in severe downslope wind flow. *J. Atmos. Sci*, **48** No. 10, 1319-1324.

Smith, R.B., 1985 On severe downslope winds. *Tellus*, **41A**, 401-415.

Thorpe, S.A., 1994 Statically unstable layers produced by overturning internal gravity waves. *J. Fluid Mech.* **260**, 333.

Winters, K.B. and Riley, J.J., 1992 Instability of internal waves near a critical level. *Dyn. Atmos. Oceans* **16**, 249-278.